

Applications of Density Functional Theory on Heavy Metal Sensor and Hydrogen Evolution Reaction (HER)

Venkatesan Srinivasadesikan, Chitra Varadaraju, Raghunath Putikam and Shyi-Long Lee

Abstract

A great effort has been devoted to develop the numerical methods to solve Schrödinger equation for atoms and molecules which help to reveal the physico-chemical process and properties of various known/unknown materials. Designing the efficient probe to sense the heavy metals is a crucial process in chemistry. And, during this energy crisis, to find the effective conversion materials for water splitting is an important approach. The density functional theory (DFT) is a powerful tool to identify such materials and made great achievements in the field of heavy metal chemosensor and photocatalysis. Particularly, DFT helps to design the chemosensor for the effective sensor applications. The universe is moving towards the exhaustion of fossil fuels in a decade and so on, DFT plays a vital role to find the green energetic alternative to fossil fuel which is the Hydrogen energy. This book chapter will focus on the application of DFT deliberately on the heavy metal sensors and hydrogen evolution reaction.

Keywords: DFT, HER, hydrogen evolution reaction, heavy metal sensor

1. Introduction

Since pronounced by Dirac in 1929 that “The underlying physical laws necessary for the mathematical theory of a large part of physics and the whole of chemistry are thus completely known, and the difficulty is only that the exact application of these laws lead to equations much too complicated to be solved” [1]. So, a great effort has been devoted to develop the numerical methods to solve Schrödinger equation for atoms and molecules which help to reveal the physico-chemical process and properties. The density functional theory has become an important tool for physicist, chemist, and material scientist. Over the past three decades, DFT has been developed successfully challenging traditional wavefunction-based methods for large scale quantum chemistry calculations. DFT has become an important method and suitable alternative to *ab initio* method as well as cheaper in terms of computational cost. The well-developed modern DFT is applicable to quantum as well as classical systems based on the theorems of Hohenberg

and Kohn [2]. The system is having N-particles allowing interactions with a given interparticle interaction, the total energy is completely derived by specification of external field $\varphi(\mathbf{r})$ using Hamiltonian and ground-state wave function. Many electron wave functions $\psi(\mathbf{r}_1, \mathbf{r}_2, \dots, \mathbf{r}_N)$ could be obtained by solving Schrödinger equation provided all the necessary information about the system. The density of single particle possibly acquired which on performing integration over any one of the single directions of coordinates of N-1 electrons,

$$\rho(\mathbf{r}) = N \int \dots \int \psi(\mathbf{r}_1, \mathbf{r}_2, \mathbf{r}_3, \dots, \mathbf{r}_N) \psi(\mathbf{r}_1, \mathbf{r}_2, \mathbf{r}_3, \dots, \mathbf{r}_N) d\mathbf{r}_2 \dots d\mathbf{r}_N \quad (1)$$

where,

$$\int \rho(\mathbf{r}) d\mathbf{r} = N \quad (2)$$

In other words, the functional of $\varphi(\mathbf{r})$ gives the ground state energy of the system. During the development of DFT, Hohenberg and Kohn Sham (HK) shown that the correspondence between external field $\varphi(\mathbf{r})$ and the single-particle density $\rho(\mathbf{r})$ and its consequence lead to the total ground state energy with the functional of $\rho(\mathbf{r})$ using the following equation,

$$E[\rho] = E_0[\rho] + \int d\mathbf{r} \varphi(\mathbf{r}) \rho(\mathbf{r}) \quad (3)$$

Moreover, Hohenberg and Kohn proved and called a second theorem which provides an energy variational principle. Further, they showed the trial density which satisfies $\int \rho(\mathbf{r}) d\mathbf{r} = N$

$$E[\bar{\rho}] \geq E_g \quad (4)$$

Here, E_g is the ground state energy. In Eq. (4), the Left Hand Side (LHS) and Right Hand Side (RHS) attain equal when $\bar{\rho}(\mathbf{r})$ is the true ground state single particle density.

In case, $E_0(\rho)$ were known for an interacting electron of a given system, then the Eqs. (3) and (4) allows to calculate the ground state energy and density of electron of any multi-electron system in a given arbitrary external field. Though, HK approach produce the total energy calculation but it does not provide any prescription for its determination. So, it is ultimate goal of a researcher to establish and develop accurate approximate functionals. Of course, in later 1990s, a number of functionals was developed to produce the experimental observations. A familiar and few density functionals are hybrid density functional B3LYP [3–5] introduced by M.J.Frisch in 1994, further gradient-corrected correlation functional: Perdew-Burke-Ernzerhof (PBE) [6] was introduced by Ernzerhof, M. in 1996, the Global Hybrid Meta-GGAs Minnesota [7–11] functionals such as M05, M06-HF, M06, M06-2X, M08-HX, M08-SO, revM06, MN15-L introduced by Donald G. Truhlar during 2005 to 2016, dispersion corrected functionals DFT-D [12], DFT-D3 [13], then the First GGA functionals were introduced by Stefan Grimme in the period of 2006–2014, moreover the another dispersion corrected method ω B97XD [14] was introduced by M. Head-Gordon in 2008. The functionals played an important role

to predict the properties of unknown materials and also explain the post-process analysis of experimental results. Selection of the method is the key in computational chemistry to achieve appropriate results.

In the past 30 years, the evolution and success of DFT for various chemical applications, emerged as the most popular electronic structure method for the chemists and plays a vital role in computational chemistry. To parameterize electronic structure theory methods and to give the guidance to chemist, nearly five different databases evolved so far *viz.*, GMTKN, MGCDB84 [15], Minnesota2015B [16], DP284 [17], and W4-17 [18]. In addition to that the W4-17-RE [19], and MN-RE [20] are two newly developed databases for reaction energies. In 2018, Peverati P et al., comprised the above mentioned databases and published it in the name of ACCDB [21]-which includes data from 16 different research groups, for a total of 44,931 unique reference data points. Now a days, data points and databases plays an important role to proceed the research further to get clear picture on history. This kind of databases will be the standard reference for the future research. In computational chemistry, the various DFT methods have been implemented and studied in several systems including chemosensor [22, 23], hydrogen evolution reaction (HER) [24–26], oxygen reduction reaction (ORR) [27, 28], oxygen evolution reaction (OER) [29], molecular machines [30, 31], DNA mutation [32–34], selective etching [35, 36], atomic layer deposition (ALD) [37, 38] etc. Although a number of applications of DFT were reported, this book chapter precisely focused on heavy metal sensor and hydrogen evolution reaction.

2. Heavy metal sensor

With the increasing population globally, there is a demand to provide clean and safe drinking water to them. However, contaminants in water at several countries/cities restrict the water supply. The contaminants most likely the heavy metals, occurring due to anthropogenic, agricultural, mining, industrial revolution etc. Commonly identified heavy metals are Hg^{2+} , Pb^{2+} , Cu^{2+} , Cd^{2+} , Cu^{2+} , which are although essential for living being but these heavy metals are toxic at higher concentrations [39]. So, it is a need to find the heavy metal sensor and this chapter will specifically focus on those sensors.

A series of 2,2'-Bipyridyl functionalized Iridium(III) complexes were synthesized by Zhao et al. [40] enabled sensing behavior towards Zn^{2+} , Cd^{2+} , Cu^{2+} ions. The modification of binding sites led to conversion of intra-ligand charge transfer (ILCT) to Ligand–Ligand Charge Transfer (LLCT) and Metal–Ligand Charge Transfer (MLCT) transition upon binding with metal ions. DFT calculations using gradient corrected correlation functional PBE1PBE and 6-31G(d,p) basis set were employed to confirm the transition mechanism using HOMO and LUMO energies of the Iridium(III) complexes with heavy metal ions. Kim et al. [41] synthesized two triphenylamine-based dyes as fluorescent probes for effective sensing of Hg^{2+} ions. The fluorescence emission band was decreased and increased on addition of Hg^{2+} ions due to metal to ligand charge transfer (MLCT) mechanism. The optimization of the dye structures was carried out at DFT level with exchange correlation functional of LDA based on PWC set. The LUMO energy levels of mono-benzoxazole and di-benzoxazole were found to be -4.61 eV and -4.74 eV, respectively. The HOMO energy levels of mono-benzoxazole and di-benzoxazole were found to be -2.51 and -2.82 eV, respectively. In this way, Anand et al. [42] reported the aminoquinoline fluorescent probe for selective and sensitive detection of Pb^{2+} and Al^{3+} ions with significant fluorescence enhancement. The fluorescence signaling was due to the inhibition of photo-induced electron transfer process and restriction of C=N isomerization. The fluorescent turn-on mechanism was understood by carrying out DFT calculations at B3LYP level. The HOMO, HOMO-1 and LUMO

energies of the probe were -5.18 eV, -5.67 eV and -2.29 eV, respectively. On complexation with Pb^{2+} , the HOMO, HOMO-1, HOMO-2 and LUMO energies were -6.18 eV, -6.42 eV, -6.95 eV and -3.69 eV respectively and for Al^{3+} , it was found to be -6.03 eV, -6.93 eV, -7.35 eV and -3.54 eV respectively. Gonzalaz et al. [43] reported the Tripodal pyrenyl-triazole probe and demonstrated citrate ion recognition with significant fluorescence enhancement. DFT calculations using B3LYP-D3/def2-TZV basis set in gas and solvent phase revealed the stable geometry of the tripodal probe as nesting type, whereas all triazole CH units bind with citrate ions. The probe also showed a remarkable chromogenic behavior from pale to deep orange seen by naked-eye which was further confirmed by DFT calculations. In 2018, Liao et al. [44] have designed and developed NiCo_2O_4 nanoplatelets modified glass carbon electrodes for detection of Pb^{2+} ions. The DFT computations were explored to calculate the adsorption bond energies of the NiCo_2O_4 nanoparticles with Pb^{2+} heavy metal ions. Pb has the largest adsorption energy of -2.78 eV with the nanoparticles and was in-line with the electrochemical experimental values. The modified glass electrodes were analyzed in real water samples and found that detection of Pb^{2+} ions was successful compared with detection of Hg^{2+} and Cu^{2+} ions. Particularly for Cu^{2+} ion sensor, Sun et al. [45] reported 1,8-diaminonaphthalene derived probe as effective fluorescence chemosensor towards Cu^{2+} ions. The fluorescence quenching was experienced due to the inhibition of intramolecular charge transfer (ICT) process and chelation enhanced fluorescence quenching (CHEQ) of paramagnetic Cu^{2+} ions. The TD-DFT calculations were performed using B3LYP/6-31(d) and LANL2DZ basis sets produced the HOMO-LUMO band gap of copper complex as 2.15 eV and the probe as 2.82 eV. This reduction in the band gap confirms the interaction of Cu^{2+} ions with the receptor. The adsorption studies explored using cetyltrimethyl ammonium bromide on Poly-L-Lysine coated Ag nanoparticles were employed at B3LYP level using 6-31 g(d) and LANL2DZ basis sets reported by Moudgil et al. [46]. The binding energy of the organic core with silver nanoparticles was found to be -0.75 eV indicates the chemisorption of pi-bonding orbitals on the Ag surface. The binding energy was observed to be reduced further 1 eV while interacting with Hg^{2+} ion which confirms the aggregation mechanism and a charge transfer through amine group. Thiocarbazone based probe was reported by Mahajan et al. [47] as multi-ions sensor for Ni^{2+} , Cu^{2+} , Co^{2+} and Cd^{2+} . The calculated stabilization energy by DFT and the observed result from the fluorescent spectra produced the same order for metal ions binding with probe. The order of the metal ion sensing was found to be $\text{Cu}^{2+} > \text{Ni}^{2+} > \text{Co}^{2+} > \text{Cd}^{2+}$. Changes in the bathochromic shift in absorption spectra and fluorescence quenching for these metal ions were due to the interaction of sulfur and hydroxyl O atoms of the probe. The binding interaction was supported by TD-DFT calculations at B3LYP level using LANL2DZ basis set. The calculated HOMO-LUMO band gap values were decreased for the metal ion-probe complex than that of probe confirms the complex formation. The real time experiment was explored with river water samples. The imidazole based receptor was reported by Khan et al. [48] to sense picric acid (donor-acceptor) for detection of toxic nitrobenzene through static quenching, Dexter electron transfer and Forster resonance energy transfer quenching mechanisms. The HOMO and LUMO orbital energies were obtained at B3LYP/6-31 g(d) level as -3.00 eV and -6.91 eV for the probe and the HOMO and LUMO energies were found to be -3.15 eV and -7.64 eV upon binding with nitrobenzene. These orbital energy values confirmed the transfer of electron from LUMO of the probe to the LUMO of nitrobenzene which is supported by the quenching mechanism. The charge transfer between the probe and the metal ion was confirmed by electrostatic potential calculation of the binding site. Moreover, the HOMO-LUMO energy gap of the probe- Co^{2+} complex was reduced to 1.86 eV well adhering to the charge transfer process. Kumar et al. [49] reported a dicarboxylic acid based receptor as turn-on fluorescent probe for detection of Hg^{2+} ions. The binding of Hg^{2+} ion takes place through the D-pi-A system by $-\text{COOH}$ and $-\text{NH}_2$

functional groups through intra-molecular charge transfer (ICT) mechanism. DFT calculations confirmed the ICT mechanism by analyzing the HOMO-LUMO energy differences. The band gap was found to be decreased for the Hg^{2+} ion complex rather than the unbound probe which confirms the host-guest interaction. Chiral CdSe nanoplatelets – L/D-cysteine as sensitive optical probe for recognition of Pb^{2+} ions was reported by Wang et al. [50]. The TD-DFT calculations at B3LYP level using LANL2DZ basis set was carried out. The results of frontier molecule orbital calculations of the HOMO and LUMO orbitals showed overlapping between the cysteine capped CdSe nanocluster and the organic core. Moreover, the reason for the transformation into chirality was observed to be the orbital coupling effect in the nanocluster. The Pb^{2+} was recognized by L-Cysteine capped CdSe nanoplatelets. The merocyanine dye based receptor [51] crystallized in monoclinic P21/n space group showed pi-pi stacking between merocyanine units. The B3LYP method was employed to optimize the geometries of the free receptor and mercuric complex. For optimization, 6-31 g(d) and LANL2DZ basis sets were used for non-metal and metal atoms, respectively. The change in the HOMO-LUMO band gap for the mercury complex than the receptor confirms the selective sensing of Hg^{2+} ion with phenolic and methoxy oxygen moieties. Modified calix[4] arene based probe was reported by Anandababu et al. [52] selectively detected Zn^{2+} ions with 240-fold fluorescence enhancement due to the imine C=N isomerization. In turn, Cu^{2+} and Hg^{2+} ions showed fluorescence quenching due to its paramagnetic and spin-orbit coupling properties. DFT studies revealed the HOMO-LUMO energy difference of unbound probe as 1.07 eV and [probe- Zn^{2+}] has a decrement to 0.15 eV, confirming the strong complexation. The luminescent metal organic frameworks (LMOFs) as nanocages to recognize Fe^{3+} and Cu^{2+} ions in trace quantity was designed and synthesized by Li et al. [53]. The fluorescent quenching activity of the nanocages was due to their weak interaction with the metal ions at N-rich sites. DFT calculations confirmed the uncoordinated N atoms in the nanocage interact weakly with the metal ions and hence the fluorescence was quenched. The other chemosensor based on Nitrogenous carbon dots impregnated on natural microcline nanostructures demonstrated a dual fluorometric response towards Fe^{3+} and Cr^{6+} metal ions was reported by Bardhan et al. [54]. The fluorescence turn OFF response was attributed by photo-induced electron transfer mechanism and was confirmed by TD-DFT calculations. The B3LYP level and 6-31 g(d,p) with RIJCOSX basis sets were utilized and revealed that the microcline structure holds the carbon dots which in turn bind with the metal ions. The possible binding site is the nitrogen atoms present in the C-dots deduced by its electrostatic potential surface calculation. The HOMO-LUMO band gap was reduced by 2.49 eV in the metal ion complexes. Carbohydrazide based colorimetric sensors for detection of multiple ions were reported by Tekuri et al. [55]. The receptors showed selectivity towards Cd^{2+} , Hg^{2+} , Pb^{2+} , Cu^{2+} and AsO_2^- ions with low detection limit. Using B3LYP functional and non-relativistic effective core potential (ECP) with LANL2DZ and 6-31 g(d,p) basis sets confirmed the binding of receptor with different metal ions as per hard and soft (Lewis) acids and bases (HSAB) theory. The hard -OH group and soft C=N group binds with complementary metal ions. The HOMO-LUMO band gap for the [receptor(s)-metal ion(s)] complexes showed a reduction in their values confirmed the binding of the respective metal ions. The novel silsesquioxane cage – porphyrin nanocomposites reportedly [56] a dual chemosensor towards fluoride and cyanide ions particularly these ions bind with the Si atoms in the cage resulted in turn on fluorescence. The microporous surface of the polymeric cage with extended conjugation was confirmed by non-local density functional theory using slit shape modeling. The extended conjugation gives a red shift in the absorption band and was confirmed by DFT calculation specifically the dropping in band gap value of the nanocomposites. In turn, the fluorescence emission was quenched in the presence of Hg^{2+} and Cu^{2+} ions due to the restricted photo-induced electron transfer process. An eco-friendly garlic

extracted alliin based silver nanoparticles was synthesized by Paw et al. [57]. This AgNPs selectively detects Hg^{2+} and Sn^{2+} ions with easily detectable color change from brown to colorless. The structure was optimized by M06-2X level with LANL2DZ and 6-31 g(d) basis sets. Ag^0 with alliin stabilizes the nanocluster with the stabilization energy of $18.4 \text{ kcal mol}^{-1}$. On interaction with Hg^{2+} and Sn^{2+} ions, alliin separated out from AgNPs with stabilization energies of $7.6 \text{ kcal mol}^{-1}$ and $8.3 \text{ kcal mol}^{-1}$, respectively. A novel N-doped diaza derivative of ovalene as nanographenes was reported by Jin et al. [58]. The N atom in the zigzag edges of ovalene favored the interaction with protons, Cu^{2+} and Fe^{2+} ions. The HOMO-LUMO band gap with 2.20 eV and 2.13 eV for diaza and ovalene nanographenes were calculated at DFT level of theory in gas phase. The N-bearing diaza nanographene showed fluorescence quenching in the presence of Cu^{2+} and Fe^{2+} ions due to intermolecular charge transfer. The aromaticity was reported by nucleus-independent chemical shift (NICS) calculations using GIAO at B3LYP/6-31G(d) level. The result shows that the NMR chemical shift has also been computed and confirmed.

3. Hydrogen evolution reaction

The Hydrogen evolution reaction ($2\text{H}^+ + 2\text{e}^- \rightarrow \text{H}_2$) is the cathodic half-cell reaction in acid-based electrolyzers. To understand the mechanism of electrocatalytic/photo-catalytic processes the density functional theory has been utilized as well as to predict and design the new catalyst for water splitting [59]. Production of hydrogen in efficient manner from water-splitting is an underpinning science to realize the hydrogen economy. The Janus nanoparticles which have the two different faces each consisting of different chemistry, size, morphology, material and further one face have the hydrophilic and another face have the hydrophobic nature introduced by de Gennes in his noble lecture [60]. In 2019, Chuan Zhao et al. [61] observed the higher hydrogen evolution reaction using Janus nanoparticle catalyst with a nickel-iron oxide interface and multi-site functionality. This nanoparticles have also been compared with benchmark platinum on carbon catalyst. The structure orientation during the hydrogen evolution reaction revealed by DFT calculations that Ni-O-Fe bridge at Ni- γ - Fe_2O_3 interface modifies the Gibbs free energy of the adsorption of the intermediate H atoms promote the HER. Moreover, the DFT result shows that the H atom adsorb on top site of O atoms in γ - Fe_2O_3 (311) or in fcc site of Ni(111) with the ΔG_{H}^* of -0.62 and -0.31 eV, respectively. The result of negative ΔG_{H} shown to be responsible for higher HER. The study displays that the Ni(111) fcc responsible for higher rate adsorption of hydrogen as well as the good amount HER. Yong K. et al. [62] investigated the NiCoP and vanadium doped NiCoP material based on the results of crystal structure, XRD, TEM and XPS. At two different places, the Co and V were replaced by Ni and produced the most stable material. The water has allowed to interact with the surface of NiCoP. Right after the dissociation of water, the produced OH and H are placed at the surface of Ni bridge and Ni hollow sites, respectively. During the process, Vanadium was doped in NiCoP and has observed to be the increased value of adsorption energy of OH and decreased water dissociation energy by 0.05 eV on the doped system. At the same time, the adsorption energy for hydrogen on the surface observed to be lower which is advantageous to desorption for hydrogen molecule from the surface and the desorption energy observed to be decreased by 0.09 eV. The DFT results well supported and further insights to the experimental observation of lower over potential and Tafel slope of NiCoVP as lower compared to NiCoP material. Dong et al. [63] used DFT tool to understand the role of sulfur vacancies on Co_9S_8 and Co_3S_4 in dissociation of water and HER. The author used the Vienna *ab initio* simulation package (VASP) for the calculation using generalized gradient approximation (GGA) using the

Perdew-Burke-Ernzerhof approach for the exchange–correlation term with the inclusion of correction as implemented in the method of Stephen Grimme. The adsorption energy for the H atom on Co_9S_8 and Co_3S_4 as observed to be -2.22 and -1.99 eV, respectively, investigated by Ford et al. The adsorption energy shows that both the surfaces are equally potential for the water splitting process. To understand the reaction kinetics, activation energy for H_2 dissociation has been calculated using Nudged Elastic Band method on Co_3S_4 and Co_9S_8 . The result shows that product of the reaction is exothermic. Moreover, the activation energy for H_2 dissociation has observed to be 0.4 eV and 1.1 eV on Co_3S_4 and Co_9S_8 , respectively. Also, the PDOS result shows the variation during the time of creation of the sulfur vacancy formation. From the PDOS result and low coordination of octahedral on Co_9S_8 surface, it can be concluded that the Co_9S_8 possibly act as a best catalyst for water splitting. While using $\text{Ni}_2\text{Mo}_3\text{N}$ [64] as electrocatalyst for hydrogen evolution reaction, the DFT studies shown the coordination of four for N-Mo, responsible for higher adsorption energy of hydrogen and responsible for HER. The adsorption energy of hydrogen atom at Ni and Mo site of $\text{Ni}_2\text{Mo}_3\text{N}$ are calculated to be -0.47 and -0.15 eV, respectively. The strong adsorption energy is expected to be the lower yield of HER. So, the active site for this surface is N rather than Ni or Mo. So, the calculated hydrogen adsorption energy was found to be in the range of -0.21 to 0.38 eV. In metal free electrocatalyst, to understand and show the interlayer electronic-coupling effect between $g\text{-C}_3\text{N}_4$ and N-graphene, the DFT calculations have been carried out particularly density of states have been computed. In the structure of $\text{C}_3\text{N}_4@\text{NG}$ hybrid shows the downshifting of valence and conduction bands resulting to Fermi level crosses the conduction band of $g\text{-C}_3\text{N}_4$ responsible and significant enhancement of electrocatalytic HER. Moreover, DGH for $g\text{-C}_3\text{N}_4$ and NG were observed to be -0.54 and 0.57 eV which shows the strong and weak, respectively, adsorption of H on the surfaces. So, both the chemical surfaces are unfavorable for HER. However, while coupling both $g\text{-C}_3\text{N}_4$ and NG have yielded good and enhanced HER activity. To understand the noble-metal-free nature of catalyst on HER, recently, noble-metal-free and earth-abundant electrocatalysts as noble-metal-free core-shell catalyst, $\text{MoS}_2/\text{Ni}_3\text{S}_2$ on Ni foam has been designed, synthesized and tested for HER. The synergistic effect of MoS_2 and Ni_3S_2 combination shown to be enhanced HER. The activation energy for H_2 dissociation on MoS_2 has observed as without barrier and negative reaction energy of 1.36 eV. It shows the Mo is the most responsible surface for HER and have the high potential values to explore by the chemist in the near future with various synergism. In this way, in 2018 Ternary Ni-S-Se Nanorod Arrays shown to be good catalyst supported by DFT for HER. The success of this selenium doped electrocatalytic performance towards HER as Se 3d orbitals were bonded to 3d orbitals of Ni and near Fermi level of s p orbitals, and was observed to be significant electron transfer between nickel and selenium atoms. The excellent performance of the catalyst due to the synergistic effect, 3D core structure, electronic modification of Se into nickel sulfide. To understand the solvent effect [65], a single or double layer water molecules are framed around the catalyst and investigated the water splitting process through simulation. The thermodynamic barrier estimated to be 0.6 eV for the H spill-over process, and it shows that the kinetics of HER was enhanced at Ni-RGO [66] synergistic point with the new active sites for the discharge of water. In 2015, Srinivasadesikan V et al. [67] demonstrated the DFT applications to find the role of Li on Lithium decorated surface of $\text{TiO}_2(101)$ anatase surface. The results observed to be the maximum of 13 Lithium adsorbed on the surface and furthermore addition of Lithium incorporated to sub-surface of TiO_2 anatase. The barrier energy for the H_2 dissociation on Li adsorbed TiO_2 surface has calculated to be 39.8 kcal/mol and for five Lithium decorated case, it has calculated to be 37.8 kcal/mol. The result of Lithium effect enormously reduced the barrier H_2 dissociation on bare TiO_2 surface which was reported [68]. Later, to understand the Ni effect on the way of doping and decorated

metal atoms on the TiO₂ surface, the DFT based first principle calculation has been carried out. Nickel doping and 3Ni metal atoms decorated on TiO₂ surface [69] has been investigated. Upon understanding the successful catalyst by theory, the same has been synthesized in the lab and shown good HER. With the arrival of new peak in between valence band and conduction band in density of states calculation on KSCN activation on NiO/TiO₂ [70] anatase surface and upon reduction of band gap further confirms the better effect of catalyst towards HER and the same has been confirmed by experiment.

With the above discussion, one can able to understand the power of DFT on various applications. Moreover, the number of unknown science will be explored by using the density functional theory in computational chemistry. Solving the chemical problems with understanding of physics through mathematical equation will be explored for new challenges in science.

Acknowledgements

The Center for Emergent Functional Matter Science of National Chiao Tung University from the Featured Areas Research Center Program within the framework of the Higher Education Sprout Project by the Ministry of Education (MOE) and the National Center for High-performance Computing are acknowledged.

Author details

Venkatesan Srinivasadesikan^{1*}, Chitra Varadaraju², Raghunath Putikam³
and Shyi-Long Lee⁴

1 Division of Chemistry, Department of Sciences and Humanities, Vignan's Foundation for Science, Technology and Research, Vadlamudi, Andhra Pradesh, India


2 Department of Chemistry, St. Joseph's College for Women, Tiruppur, Tamil Nadu, India

3 Department of Applied Chemistry, National Chiao Tung University, Hsinchu, Taiwan

4 Department of Chemistry and Biochemistry, National Chung Cheng University, Chia-Yi, Taiwan

*Address all correspondence to: vsdgun@gmail.com

IntechOpen

© 2021 The Author(s). Licensee IntechOpen. This chapter is distributed under the terms of the Creative Commons Attribution License (<http://creativecommons.org/licenses/by/3.0>), which permits unrestricted use, distribution, and reproduction in any medium, provided the original work is properly cited. 

References

- [1] Dirac, P.A.M. Proc. Roy. Soc. Ser. A, 1929, 123, 714
- [2] Hohenberg, P.; Kohn, W. Phys. Rev. 1964, 13
- [3] Becke A.D. J. Chem. Phys. 1993, 98, 5648-5652
- [4] Stephens, P.J.; Devlin, F.J.; Chabalowski, C.F.; Frisch, M.L. J. Phys. Chem. 1994, 98, 11623-11627
- [5] Stephens, P.J.; Devlin F. J.; Ashvar, C.S.; Chabalowski, C.F.; Frisch, M.J. Faraday Discuss, 1994, 99, 103-119
- [6] Perdew, J.P.; Burke, K.; and Ernzerhof, M. Phys. Rev. Lett. 1996, 77, 3865.
- [7] Zhao, Y.; Schultz, N. E.; Truhlar, D. G. J. Chem. Phys. 2005, 123, 161103.
- [8] Zhao, Y.; Truhlar, D. Theor. Chem. Acc. 2008, 120, 215-241.
- [9] Zhao, Y.; Truhlar, D. G. J. Phys. Chem. A 2006, 110, 13126-13130
- [10] Zhao, Y.; Truhlar, D. G. J. Chem. Theory Comput. 2008, 4, 1849-1868.
- [11] Yu, H. S.; He, X.; Truhlar, D. G. J. Chem. Theory Comput. 2016, 12, 1280-1293.
- [12] Grimme, S.; Antony, J.; Ehrlich, S.; Helge, K. J. Chem. Phys. 2010, 132, 154104.
- [13] Moellmann, J.; Grimme, S. J. Phys. Chem. C, 2014, 118, 7615-7621.
- [14] Chai, J.; Head-Gordon, M. Phys. Chem. Chem. Phys. 2008, 10, 6615.
- [15] Mardirossian, N.; and Head-Gordon, M. Mol. Phys., 2017, 115, 2315-2372.; Goerigk, L.; Hansen, A.; Bauer, C.; Ehrlich, S.; Najibi, A.; Grimme, S. Phys. Chem. Chem. Phys. 2017, 19, 32184-32215.
- [16] Yu, H.S.; He X.; Truhlar, D.G.; J. Chem. Theory Comput., 2016, 12, 1280-1293.; Yu, H.S.; He, X.; Li S.L.; Truhlar, D.G. Chem. Sci., 2016, 7, 5032-5051.
- [17] Hait D.; Head-Gordon, M. J. Chem. Theory Comput., 2018, 14, 1969-1981
- [18] Karton, A.; Sylvetsky, N.; Martin, J.M.L. J. Comput. Chem., 2017, 38, 2063-2075
- [19] Morgante, P.; Pevarati, R. Journal of Computational Chemistry 2019, 40, 839-848
- [20] Goerigk, L.; Hansen, A.; Bauer, C.; Ehrlich, S.; Najibi, A.; Grimme, S. Phys. Chem. Chem. Phys., 2017, 19, 32184-32215
- [21] Morgante, P.; Pevarati, R. Journal of Computational Chemistry 2019, 40, 839-848.
- [22] Sun, X.; Gao, A.; Zhang, H. Scientific Reports, 2020, 10, 711
- [23] Kumar, S.K.A.; Vijayakrishna, K.; Sivaramakrishna, A.; Brahmmananda Rao C.V.S; Sivaraman, N.; Sahoo, S.K. Inorganic chemistry, 2018, 57, 15270-15279
- [24] Huang, B.; Hart, J.N. Phys. Chem. Chem. Phys. 2020, 22, 1727-1737.
- [25] Li, H.; Xu, S.; Wang, M. Chen, Z.; Ji, F.; Cheng, K.; Gao, Z.; Ding, Z.; Yang, W. J. Mater. Chem. A, 2020, 8, 17987-17997
- [26] Li, H.; Han, Y.; Zhao, H.; Nat Commun, 2020, 11, 5437
- [27] Li, Y.; Zhai, X.; Liu, Y.; Wei, H.; Ma, J.; Chen, M.; Liu, X.; Zhang, W.; Wang, G.; Ren, F.; Wei, S. (2020)

- [28] Deng, C.; Li, F.; Tang, Q. *J. Phys. Chem. C* 2019, 123, 44, 27116-27123
- [29] Seh, Z.W.; Kibsgaard, J.; Dickens, C.F.; Chorkendor, I.B.; Nørskov, J.K.; Jaramillo, T.F. *Science* 2017, 355, 4998
- [30] Crucio, M.; Nicoli, F.; Palrinieri, E.; Folis, E.; Tabacchi, G.; Cavallo, L.; Silvi, S.; Baroncini, M.; Credi, A. *J. Am. Chem. Soc.* 2021, 143, 21, 8046-8055
- [31] Arumugamperumal, R.; Shellaiah, M.; Lai, Y.K.; Venkatesan, P.; Raghunath, P.; Wu, S.P.; Lin, M.C.; Sun, K.W.; Chung, W.S.; Lin, H.C. *Journal of Materials Chemistry C* 2021, 9, 3215-3228
- [32] Xue, J., Guo, X., Wang, X. et al. *Sci Rep* 2020, 10, 9671
- [33] Townsend, P.A.; Grayson, M.N. *Chem. Res. Toxicol.* 2021, 34, 179-188
- [34] Srinivasadesikan, V.; Sahu, P.K.; Lee, S.L. *J. Phys. Chem. B* 2011, 116, 11173-11179
- [35] Park, S.; Jung, H.; Min, K.A.; Kim, J.; Han, B. *Applied Surface Science*, 2021, 551, 149376
- [36] Wang, Y.; Zhang, H.; Han, Y.; Liu, P.; Yao, X.; Zhao, H. *Chem. Commun.*, 2011, 47, 2829-2831
- [37] Elliott, S.D.; Dey, G.; Maimiti, Y. *J. Chem. Phys.* 2017, 146, 052822
- [38] Shirazi, M.; Kessels, W.M.M.; Bol, A.A. *Phys. Chem. Chem. Phys.*, 2018, 20, 16861-16875
- [39] McDonald, R.I.; Weber, K.; Padowski, J.; Flörke, M.; Schneider, C.; Green, P.A. et al *Glob. Environ. Change*, 2014, 27, 96-105.
- [40] Zhao, N.; Wu, Y.H.; Wen, H.M.; Zhang, X.; Chen, Z.N. *Organometallics* 2009, 28, 5603-5611
- [41] Kim, B.S.; Kim, Y.S.; Kim, S.H.; Son, Y.A. *J. Nanosci. Nanotechnol.* 2010, 10, 7730-7734.
- [42] Anand, T.; Sivaraman, G.; Mahesh, A.; Chellappa, D. *Analytica Chimica Acta* 2015, 853, 596-601
- [43] Gonzalez, M.C.; Oton, F.; Espinosa, A.; Tarraga, A.; Molina, P. *Org. Biomol. Chem.* 2015, 13, 1429
- [44] Liao, J.; Zhang, J.; Wang, C.Z.; Lin, S. *Analytica Chimica Acta* 2018, 1022, 37-44
- [45] Sun, T.; Li, Y.; Niu, Q.; Li, T.; Liu, Y. *Spectrochimica Acta Part A: Molecular and Biomolecular Spectroscopy* 2018, 195, 142-147.
- [46] Moudgil, L.; Jaiswal, J.; Mittal, A.; Saini, G.S.S.; Singh, G.; Kaura, A. *Journal of Molecular Liquids* 2019, 276, 910-918
- [47] Mahajan, P.G.; Dige, N.C.; Vanajre, B.D.; Kamaraj, E.; Seo, S.Y. *Journal of Photochemistry and Photobiology A: Chemistry* 2019, 385, 112089
- [48] Khan, I.M.; Shakya, S. *ACS Omega* 2019, 4, 9983-9995
- [49] Kumar, A.; Ananthkrishnan, R.; Jana, G.; Chattaraj, P.K.; Nayak, S.; Ghosh, S.K. *Chemistry Select* 2019, 4, 1-11
- [50] Wang, X.; Hao, J.; Cheng, J.; Li, J.; Miao, J.; Li, R.; Li, Y.; Li, J.; Liu, Y.; Zhu, X.; Liu, Y.; Sun, X.W.; Tang, Z.; Delville, M.H.; He, T.; Chen, R. *Nanoscale* 2019, 11, 9327
- [51] Kumar, A.; Kumar, A.; Sahoo, P.R.; Kumar, S. *J. Mol. Struct.* 2020, 1206, 127702
- [52] Anandababu, A.; Anandan, S.; Syed, A.; Marraiki, N.; Ashokkumar, M. *Inorganica Chimica Acta* 2021, 516, 120133

- [53] Li, Y.W.; Li, J.; Wan, X.Y.; Sheng, D.F.; Yan, H.; Zhang, S.S.; Ma, H.Y.; Wang, S.N.; Li, D. Ch.; Gao, Z.Y.; Dou, J.M.; Sun, D.; *Inorg. Chem.* 2021, 60, 671–668
- [54] Bardhan, S.; Roy, S.; Chanda, D. Kr.; Ghosh, S.; Mondal, D.; Das, S.; Das, S. *Dalton Trans.*, 2020, 49, 10554
- [55] Tekuri, V.; Mohan, M.; Trivedi, D.R. *Chemistry Select* 2020, 5, 5289-5299
- [56] Majumdar, R.; Wannasiri, C.; Sukwattanasinitt, M.; Ervithayasuporn, V. *Polym. Chem.*, 2021, 12, 3391
- [57] Paw, R.; Hazarika, M.; Boruah, P.K.; Kalita, A.J.; Guha, A.K.; Das, M.R.; Tamuly, C. *RSC Adv.*, 2021, 11, 14700
- [58] Jin, E.; Yang, Q.; Ju, C.W.; Chen, Q.; Landfester, K.; Bonn, M.; Mullen, K.; Liu, X.; Narita, A. *J. Am. Chem. Soc.* 2021, 143, 10403–10412
- [59] Nemiwal, M, Gosu, V.; Zhang, T.C.; Kumar, D. *Int. J. Hydrogen Energy*, 2021, 46, 10216-10238
- [60] P.-G. de Gennes, *Angew. Chem. Int. Ed. Engl.* 31(7), 842-845 (1992)
- [61] Suryanto, B.H.R.; Wang, Y.; Hocking, R.K.; Adamson, W.; Zhao, C. *nature Comm.* | (2019) 10:5599
- [62] Jeung, Y.; Jung H.; Kim, D.; Roh, H.; Lic, C.; Han, J.; Yong, K.; *J. Mater. Chem. A*, 2021, 9, 12203-12213
- [63] Fronzi, M.; Assadi, M.H.N.; Ford, M.J.; *ACS Omega* 2018, 3, 12215-12228
- [64] Park, S.H.; Jo, T.H.; Lee, M.H.; Kawashima, K.; Mullins, C.B.; Lim, H.K.; Youn, D.H. *J. Mater. Chem. A*, 2021, 9, 4945
- [65] J.A. Gauthier, C.F. Dickens, L.D. Chen, A.D. Doyle, J.K. Nørskov, *J. Phys. Chem. C*121 (2017) 11455
- [66] Chanda, D.; Hnat, J.; Dobrota, A.S.; Pasti, I.A.; Paidar, M.; Bouzek, K. *Phys. Chem. Chem. Phys.*, 2015, 17, 26864-26874
- [67] V. Srinivasadesikan; P. Raghunath; M. C. Lin *J Mol Model* (2015) 21:142
- [68] Raghunath P, Huang WF, Lin MC (2013) *J Chem Phys* 138:154705
- [69] Lin, C.K.; Chuang, C.C.; Raghunath, P.; Srinivasadesikan, V.; Wang, T.T.; Lin, M.C. *Chemical Physics Letters*, 2017, 667, 278-283
- [70] Wanga, T.T.; Chiang, C.L.; Lin, Y.C.; Srinivasadesikan, V.; Lin, M.C.; Lin, Y.G.; *Applied Surface Science* 511 (2020) 145548.